Chapter 3

Preparation and structure of the samples

The investigation of magnetic properties in thin film multilayer systems requires a controlled preparation and a structural analysis of the samples. The magnetic properties of the characterized samples can be determined as a function of the composition and the structural parameters. The controlled deposition of thin films via Molecular Beam Epitaxy (MBE) has proved to be a suitable way of preparing well-defined magnetic layer systems. The deposition takes place under ultra high vacuum (UHV) conditions in a stainless steel chamber.

3.1 Experimental setup of the MBE chamber

A scheme of the MBE chamber which was used to deposit the layer systems investigated is given in Fig. 3.1.

The MBE chamber contains two principal parts: the preparation chamber with the electron beam evaporation module and the analysis chamber which provides different devices for structural *in-situ* analysis. To achieve a vacuum of the order of 10^{-10}mbar, the chamber is pumped in series with two turbomolecular pumps, which are pre-evacuated by a rotary pump. Additionally an ion getter pump, a titanium sublimation pump and a liquid nitrogen cold trap are used. A quadrupole mass spectrometer allows one to perform a residual gas analysis as well as leak tests with He gas.

An electron beam can be generated, controlled and maintained in a vacuum below 10^{-3} mbar. In the vacuum chamber, a well designed mechanical setup permits the generation and deflection of an electron beam onto the material to be melted or evaporated, which is then deposited onto an appropriate

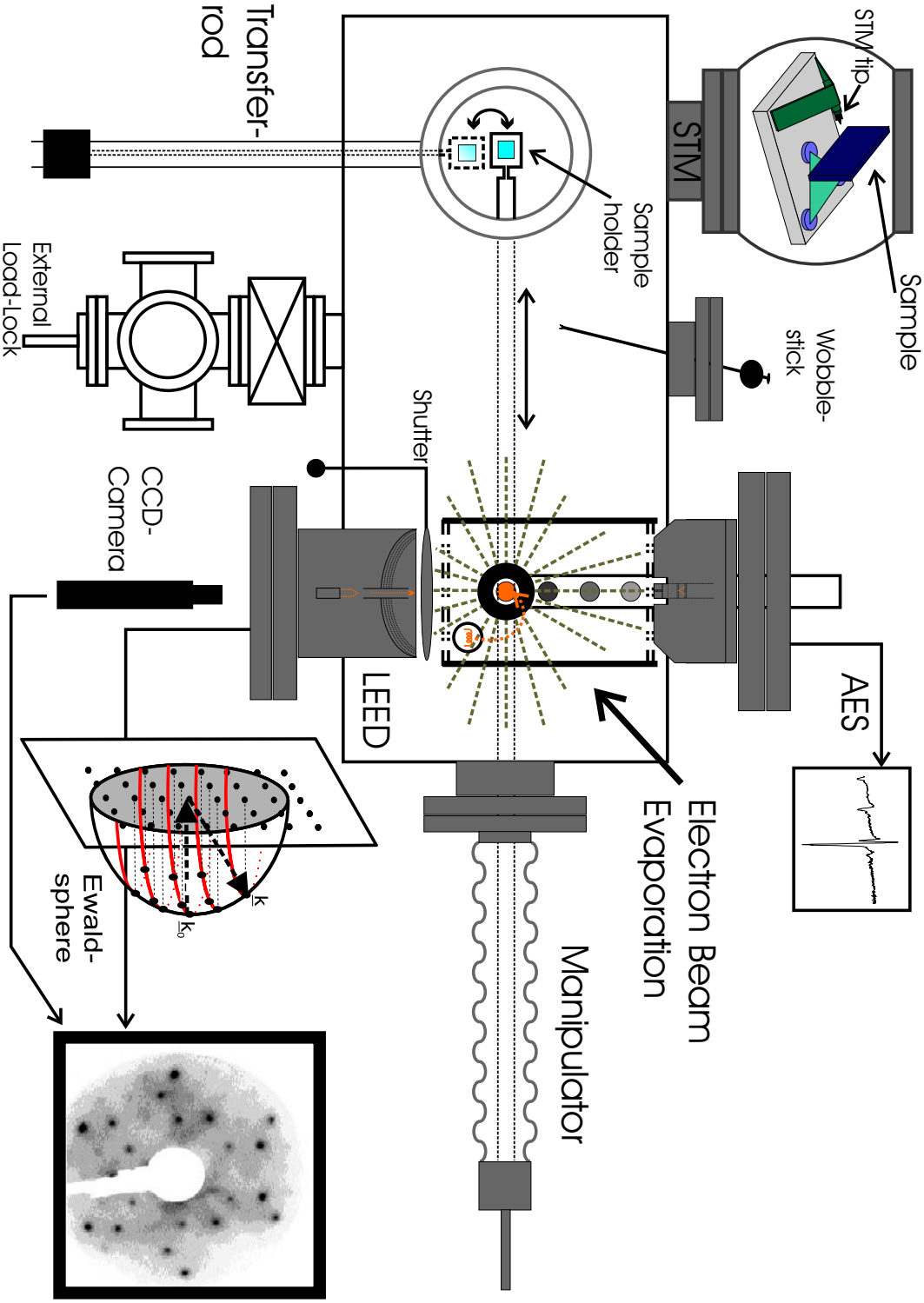

Figure 3.1: Schematic setup of the MBE chamber.

substrate. Therefore the material to be heated is usually placed in a water cooled copper crucible. The crucible has to be cooled to avoid alloying with the material when it is in its molten state. A high voltage applied between the filament (cathode) and the anode accelerates the electrons and the resulting electron beam is deflected into the crucible with an appropriate magnetic field. The rate of evaporation is monitored by a calibrated microbalance. A shutter can be used to partly cover the sample during the growth of a layer. This process can be used to prepare wedge layers. Alternatively, if several substrates are mounted on the same sample holder, side by side, the layer thicknesses of different samples in a sample set can be varied, which allows samples of different thicknesses to be prepared under otherwise identical conditions.

The sample is mounted on a sample holder which is connected to the manipulator. The latter permits motion of the sample within the chamber providing three translational and one rotational degrees of freedom. Furthermore, the sample holder is equipped with a resistance heater allowing the sample to be heated up to 1250 K.

An external interlock is provided to introduce new substrates or to take samples out while the main chamber remains evacuated. The sample transfer to the different positions for preparation and analysis of the samples is realized via a manipulator, two transfer rods (to STM and external interlock) and a wobble stick (from transfer rod to manipulator). The analysis chamber contains devices for Auger Electron Spectroscopy (AES), Low Energy Electron Diffraction (LEED), and Scanning Tunneling Microscopy (STM). The previously mentioned analysis methods will be briefly explained in the following:

- **Auger electron spectroscopy (AES)**

  The chemical purity of the samples is checked with AES [Sea72]. The method basically uses the Auger effect: if ions, electrons or high energy photons hit a surface, there is a definite probability that an electron will be knocked out of the inner shell. The vacancy is occupied by an electron from an outer shell. This transition corresponds to an energy gain, which can lead to the removal of a second electron from the outer shell. This latter electron is detected as an "Auger electron". Since these transitions originate from atomic energy levels they are element specific and the method is suitable for checking the composition of a surface and the region close to the surface. The nomenclature for the Auger transition is given by the electron shells contributing to the process; e.g. in LMM Auger transitions L- electrons are ejected from the surface

and the vacancies in the L-shells are occupied by M-electrons, causing an energy gain which is finally transferred to other M-electrons.

The intensity loss dI of the primary electron beam upon penetrating a slab of material with thickness dx is a function of the incoming intensity I_0 and the factor $\frac{1}{\lambda}$, which describes the cross section of the material, where λ is the electron mean free path. This leads to the following dependency:

$$I(x) = I_0 e^{-\frac{x}{\lambda}}. \tag{3.1}$$

This dependence between the Auger electron intensity and the thickness x of a material slab allows the determination of the amount of coverage and of the growth character. Therefore the intensity changes of the Auger signals originating from the substrate and the layer have to be compared as a function of the thickness of the layer deposited. The primary electron energy used in AES is generated by an electron gun and is of the order of magnitude of 3 to 5 keV.

The type of analyzer used is a cylindrical mirror analyzer (CMA), where the electron source for the excitation of Auger electrons is situated on the cylinder axis of the CMA. The primary electrons, generated by the electron gun, penetrate the sample and the Auger electrons can subsequently be detected by the CMA.

- **Low Energy Electron Diffraction (LEED)**

In addition to the chemical analysis via AES, the characterization of the crystal structure can be achieved with LEED [MvH79]. In this technique an electron beam of an energy between 10 and 1000 eV is scattered coherently from a crystalline surface. This energy range corresponds to a de Broglie wavelength λ of the order of magnitude of the atomic distances. An electron gun generates a collimated and monoenergetic electron beam directed at the sample. The sample is located at the focal point of a system of spherical grids and a fluorescent screen. If electrons are scattered coherently, an interference pattern of the two- dimensional lattice can be observed on the luminescent screen. The LEED pattern is an image of the surface symmetry in reciprocal space ([MvH79, Kit99]).

For constructive interference, the well known Bragg condition has to be fulfilled:

$$2d \cdot sin\theta = n\lambda, \tag{3.2}$$

where d is the distance between lattice points in a two-dimensional surface and 2θ is the angle between the incoming and the diffracted electron beams. This method is sensitive for the investigation of surfaces since the penetration length of the primary electrons is only a few monolayers. As opposed to X-ray diffraction methods, it is not sensitive to the third spatial direction, i.e. the lattice spacing perpendicular to the sample surface. The LEED pattern facilitates the determination of the two-dimensional symmetry of the crystalline surface.

- **Scanning Tunneling Microscopy (STM)**

  A surface analysis with potentially atomic resolution can be performed with a Scanning Tunneling Microscope (STM). A scheme of the STM is given in Fig. 3.1 (see also [BS92]). An atomically sharp metal tip is approached carefully to the sample surface until a tunnel current between the tip and the sample surface is detectable. To achieve a detectable current, the potential difference between the tip and the sample surface usually has to be less than 2 V. This current arises at a tip-surface distance of approximately 1 nm. Technically this requires the control of the metal tip with a precision of 0.1 to 0.01 nm in all three space directions. To provide reproducible results, the tip is mounted on piezoelectric crystals. Therefore it requires only small changes to the piezo-voltage to position the tip.

  According to Eq. 3.3, the tunneling current i is extremely sensitive to the distance between tip and surface [BS92]:

  $$i = Ke^{-A\Phi\frac{1}{2}z}. \tag{3.3}$$

  K is a constant, Φ an effective work function, z gives the height of the tip with respect to the sample surface and $A = \sqrt{[\frac{4\rho}{(2mh)}]} = 10.25\frac{1}{nm\ eV^{1/2}}$. Thus it can be estimated that a height difference of 0.3 nm, between atomic layers changes the tunneling current by a factor 400 to 1000.

Fig. 3.1 gives a schematic diagram of the positions of the different devices which are part of the MBE chamber. The evaporation unit is situated in the same part of the chamber as the AES and LEED. Both spectrometers can be moved into protected positions, so that they are not damaged during MBE growth. Additionally, the LEED screen is protected by a shutter.

The LEED as well as the Auger spectrometer can be controlled by software. The image acquisition of the LEED patterns occurs via an externally mounted

CCD camera which is controlled by a Video-LEED system. A more detailed description of the MBE chamber and its particular devices can be found in Ref. [Pol96].

3.2 Preparation of Co/CoO and Co/Au/CoO multilayer systems

Hydrogen-passivated H-Si(111)1×1 substrates, as well as $Al_2O_3(0001)$ substrates with a size of $5 \times 4 \times 0.35$ mm^3 were used for the samples which were prepared for SQUID (Superconducting Quantum Interference Device) magnetometry measurements and Low Temperature Nuclear Orientation (LTNO) measurements.

Following a well-established procedure [HCTR90], the H-Si(111) substrates were prepared *ex-situ* by wet chemical treatment in basic HF solutions as described in Ref. [GGR01]. After a final etching they were introduced into the Ultra High Vacuum (UHV) chamber.

The sapphire substrates with an rms roughness of 0.4-0.9 nm were obtained from the commercial supplier CRYSTAL in Berlin. Before introducing the Al_2O_3 substrates into the UHV chamber they were subjected to an ultrasonic bath using successively acetone and propanol. After precleaning the substrates they were immediately introduced into the chamber. Thereafter they were annealed for about one hour at a temperature of $\approx$ 850 K in a vacuum of $\approx 10^{-10}$ mbar to remove possible contaminations from the surface.

Co(16.4 nm)/Au(x nm)/CoO(2 nm) trilayers were deposited on the H-Si(111) substrates with Au layer thicknesses of x = 0.25-6.0 nm. The Co and the Au were grown at a low rate of 0.1-0.2 nm/min at a base pressure in the UHV chamber of 10^{-10} mbar and at room temperature. For the *ex-situ* investigations (X-ray diffraction and SQUID), the trilayers were capped either with a 3-4 nm thick Au overlayer or, in preparation for the LTNO experiments (see chapter 6), with a 50 (100) nm thick Ag layer, to prevent contamination in air. The 2 nm CoO layers were obtained by an *in-situ* oxidation method [GR00a] using a controlled exposure of a thin Co layer to high purity oxygen gas. This means that after depositing a 1.8 nm thick Co film, this film is exposed for 22 minutes to 1×10^{-5} mbar of high purity oxygen, which corresponds to 10000 Langmuir ($1\ L = 1.33 \times 10^{-6}$ mbar s). A detailed analysis of this preparation method, as given in Ref. [GR00a], revealed that the CoO layers obtained have a thickness of approximately 2 nm (see also Ref. [GR00b]). This method allows one to produce EB samples with extraordinarily high EB shifts and considerably improved characteristics of the magnetic behavior, and

is well suited for the preparation of complex multilayer systems. Additionally, as-prepared Co/Au/Co and CoO/Au/CoO trilayers were produced, to be subjected to LTNO measurements.

Using the previously described preparation method, two [Co(16.4 nm)/-CoO(2 nm)/Au(3.4 nm)]$_{20}$ multilayers were grown by molecular beam epitaxy on two $30 \times 15 \times 1$ mm^3 and $5 \times 4 \times 0.5$ mm^3 Al_2O_3(0001) substrates simultaneously. The large sample was prepared for neutron reflectometry experiments, while the small sample was used for comparative measurements via SQUID magnetometry. The 3.4 nm Au layers separate the exchange-coupled Co/CoO bilayers from each other and prevent any long-range magnetic interaction [GAC97, NKS$^+$00]. As described in chapter 4, it could be confirmed by SQUID magnetometry that the characteristic magnetic properties of the simple Co/CoO bilayer are preserved in the multilayer system using this particular preparation method.

3.3 In-situ characterization via AES, LEED, STM

AES

The cleanliness of the substrates and films was checked by AES and LEED (see Fig. 3.2 and Ref. [GGR01]). The chemical composition and growth of the films were investigated by AES using a primary beam energy of 3 keV. The spectrum of a single 16.4 nm Co layer is characterized by dominant Co signals at 53, 656, 716 and 775 eV (see bottom curve in Fig. 3.2a) corresponding to MVV and LMM Auger electrons. In order to analyze the chemical composition and growth of the Au layers on top of a 16.4 nm Co layer, AES spectra were recorded for Au overlayers of different thicknesses ranging from 0 to 6 nm. The spectrum of the 6 nm Au layers exhibits exclusively the most dominant characteristic Au Auger signals (see top curve in Fig. 3.2a) at 69 and 239 eV corresponding to NVV Auger electrons. For the intermediate range of increasing Au layer thicknesses the Au growth is characterized by continuously decreasing Co signals and simultaneously increasing Au signals. More quantitative information is supplied by considering the peak-to-peak height of a specific Auger signal plotted in Fig. 3.2b. For the present data, the behavior of the intensity of the 775 eV Co Auger electrons can be fitted as a function of the Au overlayer thickness d_{Au} by an exponential decay $I_{Co}(d_{Au}) = I_0\ exp(-\frac{d_{Au}}{0.74\lambda_{Co}})$ with the characteristic decay length $\lambda_{Co} = 1.35$ nm [Sea72, GGR01]. This value is in agreement with the electron mean free path $\lambda_{El} \approx 1.3$ nm for Auger

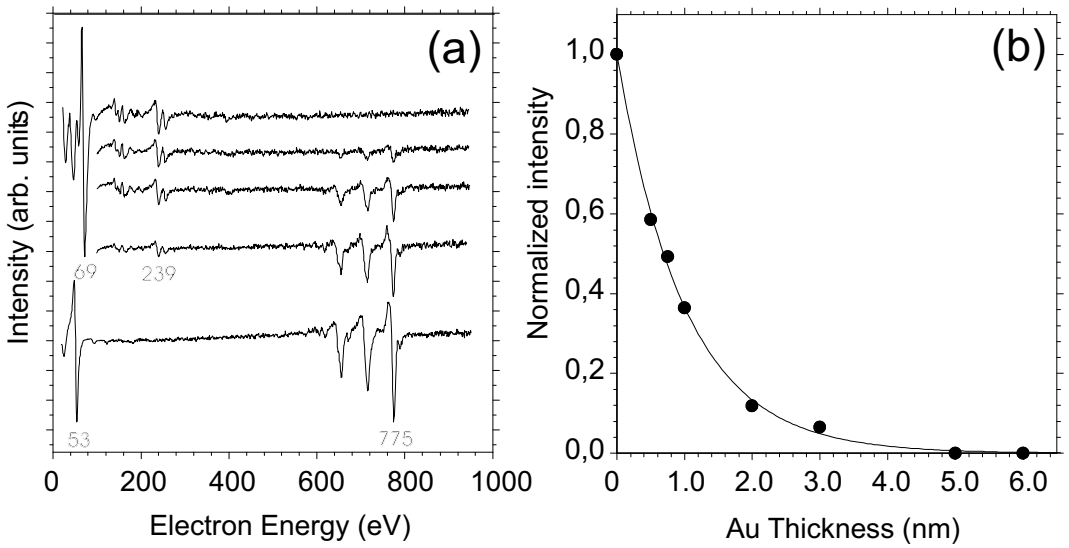

Figure 3.2: (a) Auger electron spectra for 16.4 nm Co/Au bilayers with increasing Au overlayer thickness. From bottom to top: 0; 0.5; 1; 2; and 6 nm Au. The low-energy region is shown for the bottom and top spectra (0 and 6 nm Au) only. (b) Auger peak-to-peak height of the Co LMM Auger peak at an electron energy of 775 eV versus the Au overlayer thickness. The data are normalized to the value of the Co single layer. The solid line is an exponential fit to the data.

electrons of this energy reported in the literature [SD79, Pow74]. The fit of the experimental data shown in Fig. 3.2b reveals an exponential decay expected for the deposition of a continuous Au film. However, deviations from an ideal two-dimensional layer-by-layer growth cannot be excluded. For several cases of layer-by-layer growth, Auger signals have been reported to depend linearly on thickness within each monolayer grown, which cannot be resolved in the present data. But a growth mode where large three-dimensional crystallites nucleate, so that the underlying Co layer is not completely covered until a large amount of Au has been deposited, can definitely be excluded. In the case of a dominantly three-dimensional growth mode, the Co Auger signal would vanish only for considerably higher Au overlayer thicknesses. The observed degree of attenuation of the Co signal for 2-6 nm thick Au layers, as shown in Fig. 3.2b, almost exactly agrees with the value expected for layer-by-layer growth.

In order to obtain quantitative information about the chemical composition of the CoO layer, the ratio $\frac{I(O)}{I(Co)}$ of the Auger peak-to-peak intensity of the O(503 eV) and Co (775 eV) signals is considered. A typical Auger spectrum of a CoO layer, obtained by *in-situ* oxidation of a thin Co layer [GR00a], is plotted

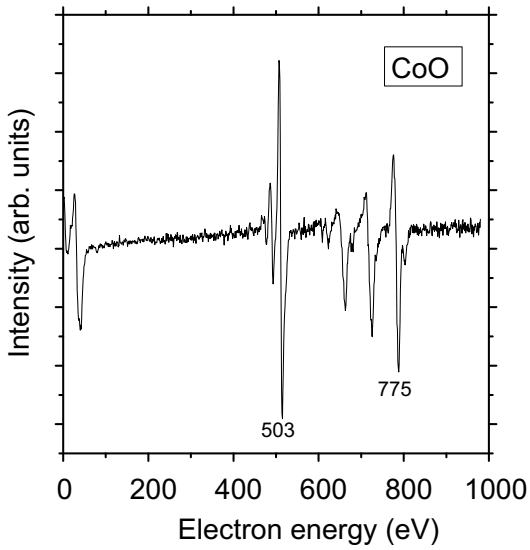

Figure 3.3: Auger electron spectrum of a CoO layer obtained by *in-situ* oxidation in 10000 L of O_2.

in Fig. 3.3. The present ratio $\frac{I(O)}{I(Co)}$ amounts to ≈ 2. An equal concentration of Co and O corresponds to an Auger intensity ratio $\frac{I(O)}{I(Co)} \approx 1.8 - 1.9$ [MI81, CVK$^+$92]. It can be concluded that the concentration of Co and O in the present sample is close to 1:1 within the electron escape depth, which amounts about 1-2 nm for the relevant Auger electron energies [VBGdB99].

LEED

The crystal structure of the sapphire substrate and the 16.4 nm Co layers deposited on top of it could be observed by LEED. The LEED patterns for the Al_2O_3 substrate (left) and for the Co layer (right) are shown in Fig. 3.4. The LEED pattern of the substrate is characterized by a threefold symmetry which is usually observed for a (0001) oriented sapphire crystal. The O^{2-} ions form a hexagonal close-packed lattice, where 2/3 of the octahedrical gaps are filled with Al^{3+} ions. This leads to the observed superstructure. The six outermost spots of the LEED pattern exhibit a sixfold symmetry. Therefore they are expected to originate from the hexagonal structure formed by the O^{2-} ions. The LEED pattern obtained from a 16.4 nm Co layer on top of the substrate (Fig. 3.4 right) exhibits a sixfold symmetry which is characteristic of fcc (111) and hcp (0001) oriented crystals.

For the case of Co layers deposited on the H-Si substrate, no LEED spots were observed.

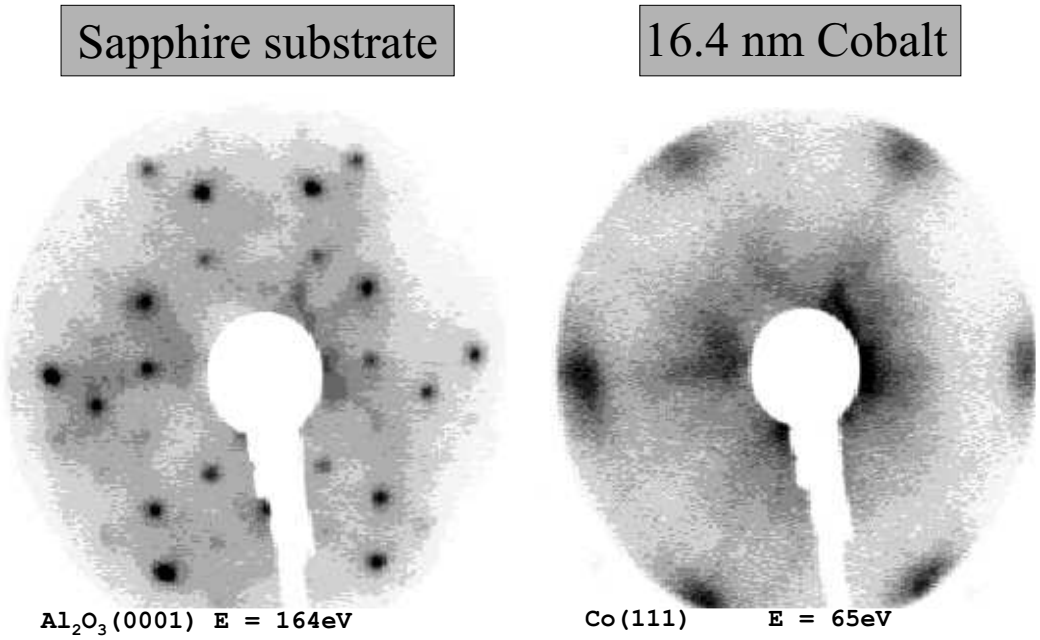

Figure 3.4: LEED pattern of the sapphire substrate (left) and the 16.4 nm Co film on top of the substrate (right).

STM

As shown from the STM images in Fig. 3.5 and Fig. 3.6 Co on both types of substrates exhibits a granular topographic structure.

Fig. 3.5 [GR00b] shows an *in-situ* STM image of the surface of a 18 nm thick Co layer. Obviously, room temperature deposition of Co an a H-Si(111) substrate yields roundly or slightly elliptically-shaped Co islands. Most of the islands touch each other but do not coalesce into a flat, uniform film. That is, the top of the Co films can be considered as a single dense layer of Co grains with a typical lateral diameter of 100±10 Å . The MBE-grown Co films are characterized by a fine grain structure with a narrow distribution of lateral grain size. The plot above the STM image represents a characteristic height profile of the Co film surface, proving that height variations along the surface and therefore also along the interface are relatively small. From the top to the edge of each island the height difference amounts only to 8 Å on average (for further details see Ref.[GR00b]). In comparison to the surface topography of Co grown on H-Si(111), the STM image in Fig. 3.6 shows an equally sized surface area of Co grown on a crystalline sapphire substrate. The prominent difference exhibited by the surface morphology of a Co layer on top of a sapphire substrate is the increased elliptical shape of the Co islands. The lateral ellipse diameters of ≈ 100 Å and ≈ 200 Å respectively indicate that

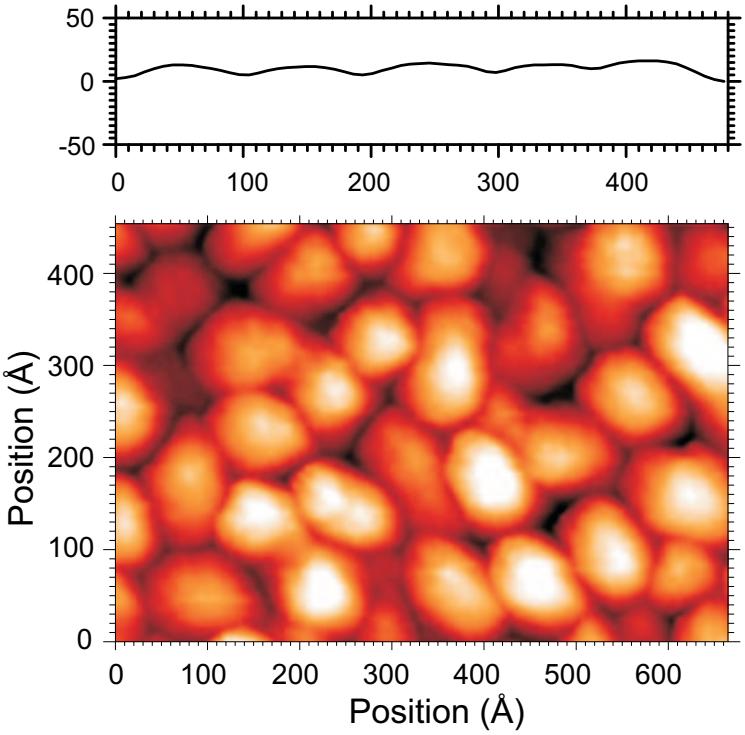

Figure 3.5: 460 Å× 670 Å STM image of an 18 nm Co film deposited on H-Si(111) [GR00b].

larger grains of single crystalline orientation are obtained for this substrate. Therefore the crystalline quality of Co on top of $Al_2O_3(0001)$, as seen from the LEED analysis, can possibly be attributed to the larger size of the Co grains and the reduced number of grain boundaries.

As already mentioned above, the 2 nm CoO layers are obtained by a controlled *in-situ* exposure of a Co layer to high purity oxygen gas [GR00a, GR00b]. STM imaging of the surface of such a Co/CoO bilayer, on top of both types of substrates, reveals no apparent changes of surface morphology compared to the pure Co layer (apart from the necessary change of the tunneling parameters). Thus it can be concluded that the CoO film consists of a single dense layer of small grains which originates from the oxidation of the top layer of Co grains in the pure film.

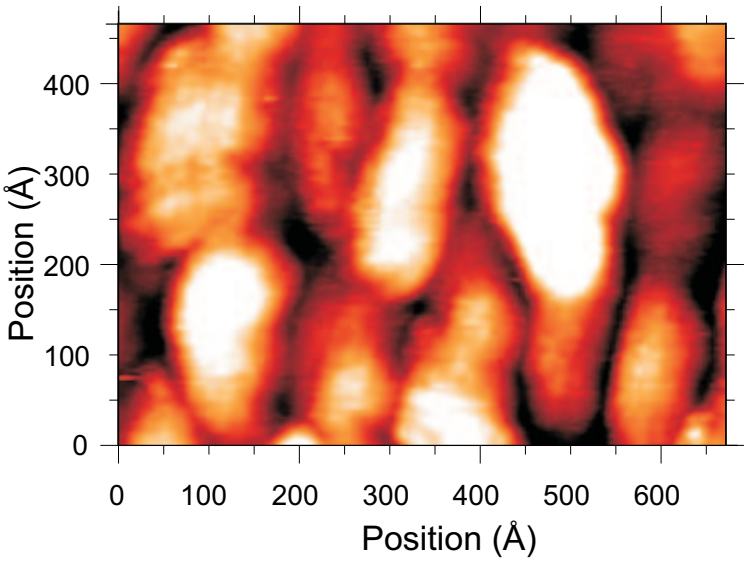

Figure 3.6: 460 Å× 670 Å STM image of an 18 nm Co film deposited on Al_2O_3.

3.4 Ex-situ characterization via X-ray diffraction and TEM

X-ray characterization

The crystalline structure of the trilayer system as well as that of the multilayer have been examined by X-ray diffraction (XRD). Fig. 3.7 shows a typical spectrum of a Co/Au bilayer deposited on a H-Si(111)1 × 1 substrate. Only two peaks at $2\Theta = 38.2°$ and $2\Theta = 44.2°$ are observed, corresponding to the fcc(111) Au and fcc(111) Co Bragg reflections, respectively. This indicates that the MBE deposition of Co onto the present substrates at room temperature leads to the growth of the fcc Co phase rather than the growth of the hcp Co phase in the thin film regime [Nai93],[dG94].

TEM characterization

The film structure of the $Co/Au/CoO$ systems as well as that of the $[Co/CoO/Au]_{20}$ were investigated by TEM (Transmission Electron Microscopy). The TEM images were made in cooperation with P. Schubert-Bischoff at the HMI. Fig. 3.8 shows a TEM micrograph of a 16.4 nm Co/ 2.25 nm Au/ 2 nm CoO trilayer capped by 4 nm Au, deposited on a H-Si(111) substrate.

The Co layer and even the very thin CoO and Au layers can be easily re-

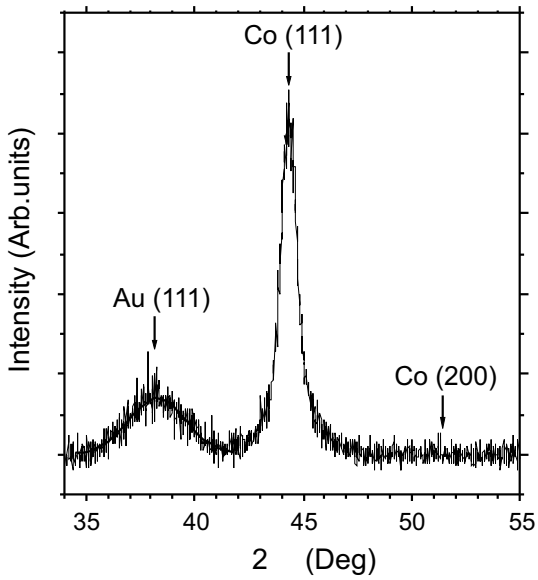

Figure 3.7: XRD pattern of a 3 nm Au/ 16.4 nm Co bilayer deposited on H-Si(111)1 $\times$ 1. The thick solid line is a fit to the Au diffraction peak at $2\Theta = 38.2°$.

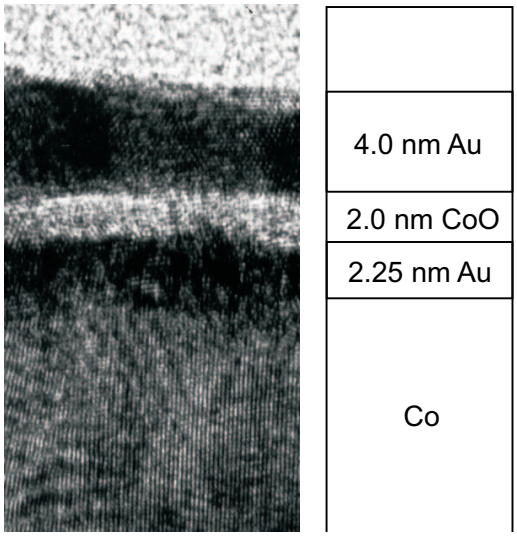

Figure 3.8: TEM micrograph showing a cross section of a 16.4 nm Co/2.25 nm Au/2 nm CoO trilayer capped by 4 nm Au. Beside the micrograph, a scheme of the multilayer structure is given.

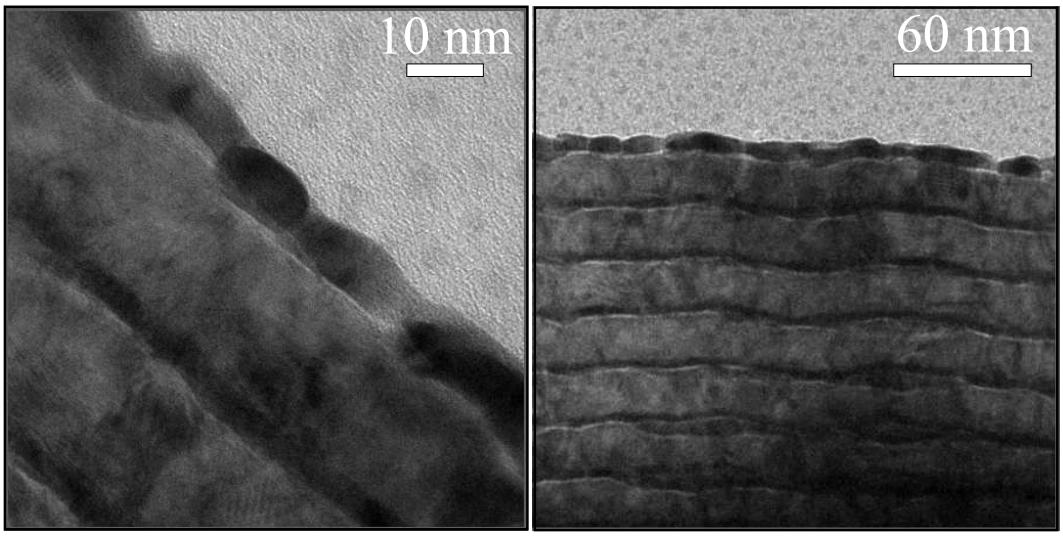

Figure 3.9: TEM image of the [Co(16.4 nm)/ CoO(2.0 nm)/ Au(3.4 nm)]$_{20}$ multilayer.

solved by the element-specific electron transmission exhibiting a high contrast for the present materials: Co (gray), CoO (light), Au (black). From this figure the interfaces in the layer system are found to be relatively sharp. In particular, the small CoO layer thickness and the complete separation from the Co layer by the 2.25 *nm* Au layer stands out in the image due to the high electron transmission through CoO.

From the TEM micrograph of the [Co/CoO/Au]$_{20}$ multilayer in Fig. 3.9 it is clear that sufficient separation of the different layers is still present even in the upper layers. Furthermore a lateral waviness can be observed, which is replicated from the bottom to the top of the multilayer.

3.5 Summary of the structural analysis

Summarizing, STM imaging reveals the present layer systems to consist of granular Co and CoO films. The Co and CoO grains were found to be significantly larger with an elliptical shape when using a sapphire(0001) substrate rather than a H-Si(111) substrate. With AES, the concentration ratio of Co and O in the CoO surfaces of the present samples was determined to be close to 1:1 within the electron escape depth. X-ray measurements determined the surface of the sample to be fcc(111) oriented. Using LEED, a sixfold symmetry was observed for the Co grown on sapphire. A sufficient separation of

the individual layers in the systems with Au layers thicker than 2.25 nm was confirmed by TEM imaging. Furthermore, the layers in the $[Co/CoO/Au]_{20}$ multilayer system exhibit a lateral waviness (on a length-scale of the order of 60 nm) which is replicated from the bottom to the top of the structure.